Measurement of the resonance parameters of the narrow orbitally excited ($L = 1$) B^0 mesons

The CDF Collaboration

Version 0.3, March 6, 2008

Abstract

We report a measurement of the masses and width of the neutral orbitally excited B mesons in decays to $B^{(*)+}\pi^-$ using 1.7 fb^{-1} of data collected by the CDF II detector at the Fermilab Tevatron. The mass and width of the narrow B_2^{*0} state are measured to be $m(B_2^{*0}) = 5740.2^{+1.7}_{-1.8}$ (stat.) ± 0.6 (syst.) MeV/c^2 and $\Gamma(B_2^{*0}) = 22.7^{+3.8}_{-3.2}$ (stat.) $^{+2.2}_{-2.3}$ (syst.) MeV/c^2 respectively. The mass difference between the narrow B_2^{*0} and B_1^0 states is measured to be $14.9^{+2.2}_{-2.5}$ (stat.) $^{+0.7}_{-1.0}$ (syst.) MeV/c^2, resulting in a B_1^0 mass of $5725.3^{+1.6}_{-2.2}$ (stat.) $^{+0.9}_{-1.1}$ (syst.) MeV/c^2. This is currently the most precise mass measurement of these states and the first measurement of the B_2^{*0} width.

The bound states of a heavy b quark with either a light u or d quark are generically referred to as B mesons. The ground $J^P = 0^-$ (B) and 1^- (B^*) states are well established [1], but the spectroscopy of the excited B states has not been well studied. The first excited state of the B meson is predicted to occur when the light quark has an orbital angular momentum of $L = 1$. This results in two isodoublets of excited states, one with a light quark angular momentum of $J_l = \frac{1}{2}$ and a total angular momentum of $\mathbf{J} = 0$ (B_0^*) or 1 (B_1^*), and another with $J_l = \frac{3}{2}$ and $\mathbf{J} = 1$ (B_1) or 2 (B_2^*) [2–7]. The four states are collectively referred to as B^{**}. The $J_l = \frac{1}{2}$ states decay to $B^{(*)}\pi$ via

an S-wave transition. Consequently, these states are expected to be very broad and have not yet been observed. The $J_l = \frac{3}{2}$ states decay to $B^{(*)}\pi$ via a D-wave transition and are expected to have widths of $10 - 20$ MeV/c^2 [3, 6]. The decay $B_1 \to B\pi$ is forbidden by angular momentum and parity conservation, while both $B_2^* \to B\pi$ and $B_2^* \to B^*\pi$ decays are allowed. Decays to a B^* are subsequently followed by $B^* \to B\gamma$, where the photon is not detected. Because of the missing photon, the observed B_1^0 and $B_2^{*0} \to B^*\pi$ peaks are shifted to a lower mass by the $B^* - B$ mass splitting of 45.78 ± 0.35 MeV/c^2 [1], resulting in an expected signal structure of three narrow $B\pi$ peaks.

Previous measurements of the neutral B_1 and B_2^* states have been made using inclusive or semi-inclusive decays which did not allow for separation of the narrow states [8–13], or were statistically limited [14]. Recently the DØ Collaboration reported resolving the neutral B_1 and B_2^* states [15], but the width of these states was not measured. In this Letter, we present a measurement of the masses of the two $J_l = \frac{3}{2}$ states, B_1^0 and B_2^{*0}, and a measurement of the width of the B_2^{*0} state. We reconstruct B^{**0} in $B^+\pi^-$ and $B^{*+}\pi^-$ decays; throughout this paper, any reference to a specific charge state implies the charge conjugate state as well. We use data collected in $p\bar{p}$ collisions at $\sqrt{s} = 1.96$ TeV by the CDF II Detector at the Fermilab Tevatron between February 2002 and January 2007, corresponding to a total integrated luminosity of 1.7 fb^{-1}.

The components of the CDF II detector [16] used for this analysis are the magnetic spectrometer and the muon detectors. The tracking system is composed of a multi-layer silicon microstrip detector [17] able to measure impact parameters with a resolution on the order of 35 μm [18]. It is surrounded by an open-cell drift chamber (COT) [19]. Both components are located inside a 1.4 T axial magnetic field. Muons are detected in planes of multi-wire drift chambers and scintillators [20] outside of the hadronic and electromagnetic calorimeters, which act as absorbers. The muon detectors cover

the pseudorapidity range $|\eta| \leq 1.0$, where $\eta = -\ln\tan(\theta/2)$ and θ is the polar angle measured from the proton direction.

A three-level trigger system is used for the online event selection. The important trigger components for this analysis are the Extremely Fast Tracker (XFT) [21], which finds tracks in the COT in the level 1 trigger, and the Silicon Vertex Trigger (SVT) [22], which at level 2 adds information from the silicon detector to the tracks found by the XFT. Two independent level 3 triggers are used in this analysis. The dimuon trigger [16] requires two tracks of opposite charge matched to track segments in the muon chambers, where the mass of the pair is consistent with the J/ψ mass. The displaced vertex trigger [23] requires two tracks with large impact parameters. Additionally, the intersection of the tracks must be displaced from the interaction point and a minimum transverse momentum, *i.e.* the momentum component perpendicular to the proton beam direction, is required for each track.

The offline reconstruction begins by reconstructing B^+ candidates in the $J/\psi K^+$, $\bar{D}^0\pi^+$, and $\bar{D}^0\pi^+\pi^+\pi^-$ decay modes with $J/\psi \to \mu^+\mu^-$ and $\bar{D}^0 \to K^+\pi^-$. Decays of $B^+ \to J/\psi K^+$ are reconstructed from the dimuon trigger data while decays of $B^+ \to \bar{D}^0\pi^+(\pi^+\pi^-)$ are reconstructed from the displaced vertex trigger data. In all three decay modes, the tracks are constrained in a 3-D kinematic fit to the appropriate vertex topology with the J/ψ and $\bar{D}^0$ masses constrained to the world average values [1]. All tracks not used to reconstruct a B^+ candidate are considered pion candidates, and their 4-momentum is added to that of the B^+ candidates to form B^{**} candidates. We search for narrow resonances in the mass difference distribution of $Q = m(B^+\pi^-) - m(B^+) - M_{\pi^-}$, where $m(B^+\pi^-)$ and $m(B^+)$ are the reconstructed invariant masses of the $B^+\,\pi^-$ pair and the B^+ candidate respectively, and M_{π^-} is the known pion mass [1].

Selection of the B^{**} candidates is done using separate neural networks for each of the three B^+ decay modes. The neural networks are based on the NeuroBayes [24] package, which combines discriminating variables into a single quantity.

We build diffferent neural networks to select B^+ in each of the three B^+ decay modes. For the decay modes $B^+ \to J/\psi K^+$ and $B^+ \to \bar{D}^0\pi^+$ channels we use the selections developed in Ref. [25]. For the decay mode $B^+ \to \bar{D}^0\pi^+\pi^+\pi^-$ we closely follow the construction of the neural networks for other two decay modes. To train this neural network we use data from the invariant mass region 5325–5395 MeV/c^2 as the background sample and the simulated B^+ events as signal sample. In all three B^+ decay modes the most important inputs to the neural networks are the impact parameter of the B^+, the projection of the distance of the B^+ decay vertex to the primary vertex on the normalized transverse momentum, the transverse momentum of the kaon or pion from the B^+ decay, and the impact parameter of the kaon or pion from the B^+ decay. We select approximately 51 500 signal events in the $J/\psi K^+$ decay channel, 40 100 in the $\bar{D}^0\pi^+$ channel, and 11 000 in the $\bar{D}^0\pi^+\pi^+\pi^-$ channel.

For the B^{**} selection, three neural networks are formulated and trained on a combination of simulated events for the signal patterns and data for the background patterns. The data for the background patterns are taken from the entire Q range of 0 to 1000 MeV/c^2. The signal contribution in the data is marginal and can be neglected during neural network training. To avoid biasing the network in the training, the simulated events are generated with the same Q distribution as the data. These neural networks use the same inputs as used by the neural networks to select B^+ mesons as well as their discriminant, and kinematic and particle identification quantities for the pion track of the B^{**} decay. The most important discriminants are the impact parameter and transverse momentum of the pion from B^{**} decay and the output of the B^+ neural network.

For the final B^{**} selection we select on the number of candidates per event and on the output of the neural networks. The requirement on the number of candidates is fixed to be the same for all three B^+ decay channels, and requires fewer than six B^{**} candidates in an event. After selecting on the number of candidates, the cut on

the neural network output is chosen to maximize $N_{MC}/\sqrt{N_{data}}$. The optimization is done by counting the number of Monte Carlo signal events N_{MC} and the number of background events in the data N_{data} in the Q signal region of 200 to 400 MeV/c^2 for a given cut on the network output. In this analysis, we combine the B^{**} events for all three B^+ decay channels and use this combined Q distribution to measure the B^{**} properties. Thus, we optimize the B^{**} selection for each B^+ decay channel using the combined significance, which is a function of all three network outputs. The resulting combined Q distribution is shown in Figure 1.

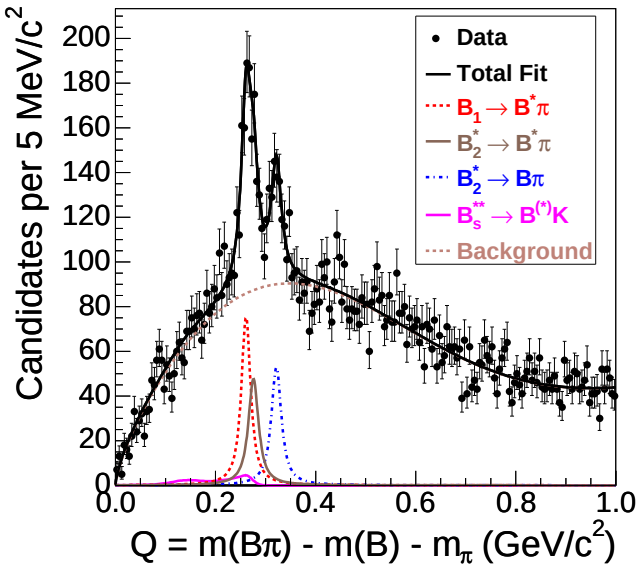

Figure 1: Invariant mass distribution $Q = m(B^+\pi^-) - m(B^+) - M_{\pi^-}$ for exclusive B^+ decays. The fit is described in the text. Curves are shown separately for the background, the B_s^{**} reflections, and the three B^{**} decay modes.

We perform an unbinned maximum-likelihood fit to the combined Q distribution. The B^{**} signal structure is interpreted as the three decays $B_1^0 \to B^{*+}\pi^-$, $B_2^{*0} \to B^+\pi^-$, and $B_2^{*0} \to B^{*+}\pi^-$, with $B^{*+} \to B^+\gamma$. Because of the missing photon in decays through B^*, we expect a total of three narrow B^{**} signal peaks. Each peak is modeled by a non-relativistic fixed-width Breit-Wigner distribution convoluted with

the detector resolution model. The detector resolution as a function of Q is determined from simulation and modeled by two Gaussian distributions, a dominant narrow core of an ~ 2 MeV/c^2 width and a small broad component of an ~ 4 MeV/c^2 width for the tails.

The current sample of data has insufficient statistics to fit for all signal parameters. We fit for the Q value of the $B_2^{*0} \to B^+\pi^-$ decay, the mass difference between the B_1^0 and B_2^{*0} states, the width of the B_2^{*0}, and the number of events in the B_1^0 and $B_2^{*0} \to B^+\pi^-$ peaks. Other parameters are imposed as part of the fit and taken either from previous measurements or from theoretical predictions. These are: the energy of the B^* photon, $E(\gamma) = 45.78 \pm 0.35$ MeV/c^2 [1]; the ratio of the B_1^0 and B_2^{*0} widths, $\frac{\Gamma(B_1^0)}{\Gamma(B_2^{*0})} = 0.9 \pm 0.2$ [3]; the ratio of the B_2^{*0} branching fractions, $\frac{BR(B_2^{*0} \to B^+\pi^-)}{BR(B_2^{*0} \to B^{*+}\pi^-)} = 1.1 \pm 0.3$, which is based on observations of the charm sector [13].

We also expect reflections from $B_s^{**0} \to B^+K^-$ decays in the B^{**} Q distribution when the kaon is mistakenly assigned the pion mass. The shape of this reflection is determined by using simulations from the study of the B_s^{**} states [25] and is a fixed component of the fit. The number of B_s^{**0} events expected in the B^{**} distributions is also determined from [25] and enter the fit as Gaussian constraints with a 50% uncertainty assigned. In this data sample we expect 24 B_{s1}^0 events and 62 B_{s2}^{*0} events.

The background is modeled by a power law times an exponential. The flattening of the background at high Q values ($Q > 700$ MeV/c^2) is modeled by a small fixed shape, also chosen to be a power law times an exponential. Tests of the fit model on randomly generated samples show a small fit bias on the B^{**} signal parameters, which is included as a systematic uncertainty.

The result of this fit to the combined data is shown in Figure 1. The χ^2 probablity of the fit is 73% in the range $Q \in [0, 500]$ MeV/c^2. The following parameters are measured for the B_1^0 and B_2^{*0}:

$$m(B_2^{*0}) - m(B^+) - M_{\pi^-} = 321.5^{+1.7}_{-1.8}\ (\text{stat.})\ ^{+0.5}_{-0.4}\ (\text{syst.})\ \text{MeV}/c^2,$$

$$m(B_2^{*0}) - m(B_1^0) = 14.9^{+2.2}_{-2.5}\ (\text{stat.})\ ^{+0.7}_{-1.0}\ (\text{syst.})\ \text{MeV}/c^2, \text{ and}$$

$$\Gamma(B_2^{*0}) = 22.7^{+3.8}_{-3.2}\ (\text{stat.})\ ^{+2.2}_{-2.3}\ (\text{syst.})\ \text{MeV}/c^2.$$

The signal is consistent with theoretical predictions [5, 7] including those entered as Gaussian constraints in the likelihood. The number of events are $N(B_1^0) = 503^{+75}_{-68}$ (stat.) $^{+87}_{-83}$ (syst.), $N(B_2^{*0} \to B^+\pi^-) = 385^{+48}_{-45}$ (stat.) $^{+29}_{-27}$ (syst.), and $N(B_2^{*0} \to B^{*+}\pi^-) = 351^{+48}_{-45}$ (stat.) $^{+29}_{-26}$ (syst.). Using the mass of the B^+ [1] and the correlations between the fit parameters, the absolute masses of the B_1^0 and B_2^{*0} are:

$$m(B_2^{*0}) = 5740.2^{+1.7}_{-1.8}\ (\text{stat.})\ \pm 0.6\ (\text{syst.})\ \text{MeV}/c^2 \text{ and}$$

$$m(B_1^0) = 5725.3^{+1.6}_{-2.2}\ (\text{stat.})\ ^{+0.9}_{-1.1}\ (\text{syst.})\ \text{MeV}/c^2.$$

Sources of systematic uncertainty on the mass differences, width, and yield measurements include: the mass scale, assumptions entered as Gaussian constraints in the fit, fit model bias, the choice of background and resolution models, and the existence of B^{**} broad states. The effect of each systematic is summarized in Table 1.

To determine the mass scale uncertainty, we compare CDF II measured Q values of the D^*, Σ_c^0, Σ_c^{++}, Λ_c^*, and $\psi(2S)$ hadrons with the world average Q values [1]. We reconstruct the decays $D^{*+} \to D^0\pi^+$ with $D^0 \to K^+\pi^-$, $\Sigma_c^0 \to \Lambda_c^+\pi^-$, $\Sigma_c^{++} \to \Lambda_c^+\pi^+$, and $\Lambda_c^{*+} \to \Lambda_c^+\pi^+\pi^-$, all with $\Lambda_c^+ \to pK^-\pi^+$, and $\psi(2S) \to J/\psi\pi^+\pi^-$ with $J/\psi \to \mu^+\mu^-$. The Q value dependence of this systematic uncertainty is modeled with a linear function, which is evaluated at the B^{**} Q values to estimate the systematic uncertainty. This is a small contribution to the systematic uncertainty.

Assumptions made in the fit are included as Gaussian constraints added to the likelihood. Thus, the systematic uncertainty due to these assumptions is part of the fit uncertainty on each parameter. To separate the statistical and systematic components

of the fit uncertainty, we refit the data with the constrained parameters fixed. The uncertainty on each parameter from this fit is purely statistical. To determine the systematic contribution to the fit uncertainty, we subtract in quadrature the uncertainties for the two fits to data, one with the constrained parameters floating and one with them fixed. Assumptions in the fit are the largest systematic uncertainty on all parameters.

To estimate the uncertainty due to the choice of background or resolution models, we generate pseudo-experiments using an alternate background parameterization or increased resolution width. From comparisons of the detector resolution in data and Monte Carlo for the $\psi(2S)$ sample, we expect the Monte Carlo to underestimate the resolution by no more than 20%. Each pseudo-experiment is modeled by both the default fit and the fit with an alternate background model or increased resolution width. We then take the difference between the parameter values in the varied fit and the default fit as the systematic uncertainty due to the model. We fit the distribution of pseudo-experiment differences with a Gaussian, and take the mean of the Gaussian as the systematic uncertainty. The uncertainty due to these effects is relatively small.

PRELIMINARY ADDITION!! Two broad $J_l = \frac{1}{2}$ B^{**} states are predicted but have not yet been observed. To account for the possible effect of these broad states on our measurement of the narrow B^{**} parameters, we add two broad Breit-Wigner shapes to our background model. These states are fixed to have the same width, which is varied between 50 and 200 MeV/c^2. The masses of the states are varied within the range 240 to 360 MeV/c^2, the region around the narrow B^{**} peaks. We refit the data for various masses and widths of the broad states, with the normalizations of the broad Breit-Wigners as additional parameters in the fit model. We then take the largest variation in the narrow B^{**} parameters from any configuration of broad states as the systematic uncertainty due to the B^{**} broad states (ADJUST THIS AS NECESSARY). The largest effect is from relatively narrow 50 MeV/c^2 broad states

Table 1: Systematic uncertainties of the B^{**0} parameters. Each row corresponds to one source of systematic uncertainty. The columns show the resulting uncertainties for the five B^{**} signal parameters. Uncertainties on the mass difference and width parameters are in units of MeV/c^2.

Source	$Q(B_2^{*0})$	$\Gamma(B_2^{*0})$	$m(B_2^{*0}) - m(B_1^0)$	$N(B_2^{*0} \to B^+\pi^-)$	$N(B_1^0)$
Mass scale	± 0.05		± 0.003		
Fit constraints	$^{+0.35}_{-0.29}$	$^{+2.09}_{-1.45}$	$^{+0.65}_{-0.94}$	$^{+26.5}_{-23.4}$	$^{+85.6}_{-71.7}$
Fit bias	$^{+0.0}_{-0.12}$	$^{+0.44}_{-0.0}$	$^{+0.0}_{-0.21}$	$^{+11.4}_{-0}$	$^{+15.2}_{-0}$
Resolution	± 0.001	$^{+0.0}_{-0.40}$	$^{+0.0}_{-0.003}$	$^{+0}_{-1.1}$	$^{+0}_{-2.0}$
Background	$^{+0.24}_{-0.0}$	$^{+0.0}_{-1.63}$	$^{+0.16}_{-0.0}$	$^{+0}_{-12.1}$	$^{+0}_{-40.8}$
Broad states					
Total	$^{+0.43}_{-0.32}$	$^{+2.14}_{-2.22}$	$^{+0.67}_{-0.96}$	$^{+28.8}_{-26.4}$	$^{+86.9}_{-82.5}$

which sit directly beneath the narrow B^{**} states.

In summary, using the three fully reconstructed decay modes of $B^+ \to J/\psi K^+$, $B^+ \to \bar{D}^0\pi^+$, and $B^+ \to \bar{D}^0\pi^+\pi^+\pi^-$, we observe the two narrow B^{**0} states in the decays $B_1^0 \to B^{*+}\pi^-$ and $B_2^{*0} \to B^{(*)+}\pi^-$. This is the most precise measurement of the narrow B^{**0} states to date. This is also the first measurement of the B_2^{*0} width.

We thank the Fermilab staff and the technical staffs of the participating institutions for their vital contributions. This work was supported by the U.S. Department of Energy and National Science Foundation; the Italian Istituto Nazionale di Fisica Nucleare; the Ministry of Education, Culture, Sports, Science and Technology of Japan; the Natural Sciences and Engineering Research Council of Canada; the National Science Council of the Republic of China; the Swiss National Science Foundation; the A.P. Sloan Foundation; the Bundesministerium für Bildung und Forschung, Germany; the Korean Science and Engineering Foundation and the Korean Research Foundation; the Science and Technology Facilities Council and the Royal Society, UK; the Institut National de Physique Nucleaire et Physique des Particules/CNRS; the Russian Foundation for Basic Research; the Comisión Interministerial de Ciencia y Tecnología, Spain; the European Community's Human Potential Programme; the Slovak R&D Agency;

and the Academy of Finland.

References

[1] W. M. Yao *et al.* (Particle Data Group), J. Phys. G **33**, 1 (2006).

[2] E. J. Eichten, C. T. Hill, and C. Quigg, Phys. Rev. Lett. **71**, 4116 (1993); E. J. Eichten, C. T. Hill, and C. Quigg, FERMILAB-CONF-94/118-T (1994).

[3] A. F. Falk and T. Mehen, Phys. Rev. D **53**, 231 (1996).

[4] N. Isgur, Phys. Rev. D **57**, 4041 (1998).

[5] D. Ebert, V. O. Galkin, and R. N. Faustov, Phys. Rev. D **57**, 5663 (1998) [Erratum-ibid. D **59**, 019902 (1999)].

[6] A. H. Orsland and H. Hogaasen, Eur. Phys. J. C **9**, 503 (1999).

[7] T. Matsuki, T. Morii, and K. Sudoh, Prog. Theor. Phys. **117**, 1077 (2007).

[8] R. Akers *et al.* (OPAL Collaboration), Z. Phys. C **66**, 19 (1995).

[9] P. Abreu *et al.* (DELPHI Collaboration), Phys. Lett. B **345**, 598 (1995).

[10] D. Buskulic *et al.* (ALEPH Collaboration), Z. Phys. C **69**, 393 (1996).

[11] M. Acciarri *et al.* (L3 Collaboration), Phys. Lett. B **465**, 323 (1999).

[12] A. A. Affolder *et al.* (CDF Collaboration), Phys. Rev. D **64**, 072002 (2001).

[13] Z. Albrecht *et al.* (DELPHI Collaboration), DELPHI 2004-025 CONF 700, contributed paper to ICHEP 2004, Beijing.

[14] R. Barate *et al.* (ALEPH Collaboration), Phys. Lett. B **425**, 215 (1998).

[15] V. M. Abazov *et al.* (D0 Collaboration), arXiv:0705.3229 [hep-ex].

[16] D. Acosta *et al.* (CDF Collaboration), Phys. Rev. D **71**, 032001 (2005).

[17] C. S. Hill, Nucl. Instrum. Methods A **530**, 1 (2004); A. Affolder *et al.*, Nucl. Instrum. Methods A **453**, 84 (2000); A. Sill, Nucl. Instrum. Methods A **447**, 1 (2000).

[18] A. Bardi *et al.*, Nucl. Instrum. Methods Phys. Res. A **485**, 178 (2002).

[19] T. Affolder *et al.*, Nucl. Instrum. Methods A **526**, 249 (2004).

[20] G. Ascoli *et al.*, Nucl. Instrum. Methods A **268**, 33 (1988).

[21] E. J. Thomson *et al.*, IEEE Trans. Nucl. Sci. **49**, 1063 (2002).

[22] W. Ashmanskas *et al.*, Nucl. Instrum. Methods A **518**, 532 (2004).

[23] A. Abulencia *et al.* (CDF Collaboration), Phys. Rev. Lett. **96**, 191801 (2006).

[24] M. Feindt, arXiv:physics/0402093 (2004); M. Feindt and U. Kerzel, Nucl. Instrum. Methods A **559**, 190 (2006).

[25] T. Aaltonen *et al.* (CDF Collaboration), Phys. Rev. Lett. **100**, 082001 (2008).